Parametric Imaging of Rat Mammary Tumors In Vivo for the Purposes of Tissue Characterization

Michael L. Oelze, PhD, James F. Zachary, DVM, PhD, William D. O'Brien, Jr, PhD

Objective. To estimate the average scatterer properties from ultrasonic backscatter in tissues for evaluating differences between neoplastic and healthy tissues. ***Methods.*** Parametric images of 8 retired breeder rats in which spontaneous mammary tumors had developed were created by superimposing color-coded pixels related to the estimated average scatterer properties on conventional gray scale B-mode images. ***Results.*** The images showed a distinct difference between the tumors and surrounding healthy tissues. Analysis of the average scatterer diameters and acoustic concentrations showed a statistically significant difference ($P < .05$) between estimates inside and outside the tumors for most of the cases. Scatterer sizes inside the tumors were on average 30% larger than scatterer sizes in surrounding normal tissues. A feature analysis plot showed that there was a distinct difference between results obtained inside and outside the tumors. ***Conclusions.*** Parametric imaging that uses estimates of scatterer properties in tissues may lead to detection and characterization (diagnosis) of diseased tissues on conventional sonographic scanning systems. ***Key words:*** frequency-dependent backscatter; parametric imaging; quantitative imaging; rat mammary tumor.

Abbreviations
RF, radio frequency; ROI, region of interest

Received April 2, 2002, from the Bioacoustics Research Laboratory, Department of Electrical and Computer Engineering (M.L.O., W.D.O.), and Department of Veterinary Pathobiology (J.F.Z.), University of Illinois at Urbana-Champaign, Urbana, Illinois. Revision requested May 17, 2002. Revised manuscript accepted for publication June 26, 2002.

We thank James P. Blue and Rita J. Miller, DVM, for technical assistance. This work was supported by National Institutes of Health grants CA09067 and CA79179.

Address correspondence and reprint requests to Michael L. Oelze, PhD, Bioacoustics Research Laboratory, Department of Electrical and Computer Engineering (M.L.O., W.D.O.), University of Illinois at Urbana-Champaign, 405 N Mathews Ave, Urbana, IL 61801.

Standard B-mode images of living tissues created with a clinical sonographic scanning system are made from radio frequency (RF) echo signals. The RF echo signals are created by reflections from interfaces between acoustically different regions and by incoherent scattering from tissue microstructures. The RF echoes contain frequency-dependent information about the smaller-scale structures (less than the wavelength) in the tissues. Generally, processing of conventional B-mode sonographic images removes the frequency-dependent information. Clinical B-mode images are good at displaying large-scale structures (larger than the wavelength), but to display and quantify the smaller-scale structures of tissues, the frequency-dependent information must be used. The tissue microstructure can be quantified by examining the frequency-dependent acoustic backscatter.[1–6]

The resolution of typical sonographic imaging devices ranges from hundreds of micrometers to centimeters. For typical sonographic imaging devices, ultrasonic backscatter RF spectral information offers the possibility of extending the resolution of the tissue microstructure to tens of micrometers in a statistical sense. Estimates of scatterer properties (subwavelength in size) from the RF signal spectrum can be incorporated into enhanced B-mode images called parametric images. Parametric images are constructed by converting estimates of scatterer properties to color-coded pixels in an image as opposed to B-mode imaging, which converts the envelope-detected RF signal to a gray scale image. The parametric images may display tissue microstructure not resolved by conventional B-mode images. The extension in resolvable microstructure has the potential to improve the diagnostic capability of sonographic imaging.

Ultrasonic backscattering techniques have been used to characterize different aspects of microstructure in biological tissues. Specifically, backscatter has been used to extract the average sizes and acoustic concentrations of random scatterers in biological tissues. Feleppa et al[7] used frequency-dependent backscatter to quantify the scatterer sizes and acoustic concentration of ocular tumors. Lizzi et al[8] used the same techniques in examining the structure of the liver, whereas Insana et al[5] used backscatter techniques to parameterize renal tissues. Numerous other experiments and detailed scattering models have been developed to help in understanding the nature of backscattered ultrasound from biological tissues.[9]

The frequency dependence of backscatter from tissues has been used to enhance existing sonographic images.[10–14] In previous works, often the shape of the scattered power spectrum with frequency was assumed to be linear so that a line could approximate the power spectrum. Different regions with different scattering properties would then have their respective, possibly unique, slope and intercept parameters that were extracted from the scattered power spectrum. In articles by Lizzi et al[13] and Feleppa et al,[12] parametric images were formed by color coding pixels in an image with the slope and intercept parameters of the power spectrum at the region of the pixels. In the work of Topp et al,[14] the parametric images were formed by superimposing small boxes (regions of interest) containing the values of the spectral slope in different areas of interest. The goal of these studies was to use the parametric images to differentiate between diseased and healthy tissues.

This study was an extension of the work by Topp et al[14] to characterize tissues from the frequency-dependent backscatter. In this study, parametric images were created that were enhanced by associating specific regions in a tissue with their average scatterer size and acoustic concentration. The assumptions of linear frequency dependence of the scattered power spectrum were only approximations to the true frequency dependence. The nonlinear frequency dependence, if modeled correctly, can lead to better estimates of specific scatterer properties. Enhancing existing B-mode images with quantified physical properties of the average tissue microstructures may lead to improved diagnosis of diseased tissue. Parametric images have been constructed for test phantoms and for preliminary studies with tissues by using estimates of the scatterer properties such as the average scatterer size and acoustic concentration.[15,16] The average scatterer sizes and acoustic concentrations are values that may be related to microscopic optical histologic evaluation. A proper understanding of the relationship between the scatterer properties and histologic structure will enable the models to be tested for their validity and will improve the ability of ultrasound to show certain diseased tissue.

Materials and Methods

Theory

Acoustic scattering theories for biological tissues assume that the tissues can be modeled as inhomogeneous fluids.[17] Scattering occurs when an acoustic wave propagates across a region that has different impedance relative to the surrounding tissue or fluid. Tissue microstructures, such as glands, collagen bundles, and transition zones between different microstructures, are hypothesized to be scattering-type particles or regions with acoustic impedances different from those of surrounding tissues. In many cases, a sphere, a cylinder, or some simple geometric configuration can approximate the scattering particle or region. Under simple approximations of the shape of the scatterer, if the size of the scattering region is on the order of the wavelength of sound, then the pattern of the scattered signal is well

known.[18] In addition, the size and shape of the scattering region determine the magnitude at which a specific frequency of sound will be scattered.

Acoustic signals backscattered from biological tissues contain information about the size, shape, number, and relative impedance of the scattering regions within the tissues. Typically, at any instant in time, the backscattered signal will be a superposition of wavelets scattered from numerous small structures confined within the volume of insonified tissue. The backscattered signal is, therefore, modeled as a statistical distribution of scatterers in size and acoustic concentration. The frequency dependence of the backscattered signal will be dependent on the average properties (size, shape, number, compressibility, and density) of the scatterers within the insonified region relative to the compressibility and density of the medium surrounding the scatterers.

The scatterer property estimates can be made by comparing the backscattered power spectrum of the RF signal gated from each region of interest (ROI) with a theoretical backscattered power spectrum. The backscattered power spectrum is related to the magnitude squared of the Fourier transform of the gated RF signal. The theoretical backscattered power spectrum is modeled from a three-dimensional spatial autocorrelation function describing the shape and distribution of scatterers in the medium.[11,19] If the scattering particles are assumed to be of a particular shape or form and to be randomly distributed (incoherent scattering), then for simple geometric shapes, i.e., spheres or cylinders, closed-form solutions for the spatial autocorrelation function can be obtained. From the closed-form solutions of the spatial autocorrelation function, closed-form solutions for the theoretical backscattered power spectrum can be calculated. The theoretical backscattered power spectrum (W_{theor}) is given by[5]

$$W_{\text{theor}}(f) = C(a_{\text{eff}}, n_z) f^4 F(f, a_{\text{eff}}), \quad (1)$$

where f is the frequency (megahertz); C is a constant depending on the average effective radius, a_{eff}, of the scatterers (millimeters) and the average acoustic concentration, n_z, of scatterers (cubic millimeters); and F is called the form factor[15,19] and is a function of the frequency and average effective scatterer radius.

The form factor describes frequency dependence of scattering based on the shape and internal makeup of the scatterer in the tissue. An important consideration for accurately estimating scatterer properties is the appropriate choice of the form factor. The Gaussian form factor has been used to model the scattering properties of many soft tissues.[2,4,8,13,17,19] The Gaussian form factor represents a spherical scatterer whose impedance varies continuously with the surrounding tissues instead of a sharp impedance discontinuity as a rigid or fluid-filled sphere scatterer might have. Furthermore, the Gaussian scatterer would have an effective radius related to the impedance distribution of the scatterer, unlike the definite radius describing a spherical shell or fluid-filled sphere. Comparison between measured form factors of the tissues and several possible theoretical form factors showed that the Gaussian best described the backscatter from mammary tumors in the rats. The Gaussian form factor is given by

$$F_{\text{gauss}}(f) = e^{-12.3 f^2 a_{\text{eff}}^2}. \quad (2)$$

The constant in Equation 2 normalizes the form factor, assuming a speed of sound in the tissue of interrogation of 1540 m/s, so that the effective scatterer radius represents the width of the –6-dB edge of the Gaussian function.[8]

Typical backscatter measurements from tissue volumes are made by choosing an ROI and gating the backscattered RF signal corresponding to the ROI. The effects of the gating function (windowing function) and beam pattern of the transducer are needed to properly model the backscattering measurement. Incorporating the gating function (Hanning window) and beam pattern effects in the development of the model normalizes the theoretical backscattered power spectrum. Lizzi et al[13] combined the effects of the gating function and the beam pattern, giving a theoretical power spectrum with the Gaussian form factor to give

$$W_{\text{theor}}(f) = \frac{185 L q^2 a_{\text{eff}}^6 n_z f^4}{\left[1 + 2.66(fqa_{\text{eff}})^2\right]} e^{-12.3 f^2 a_{\text{eff}}^2}, \quad (3)$$

where q is the ratio of aperture radius to distance from the ROI.

Typically, an ROI is made up of a number of parallel gated A-lines of the same length. The backscattered power spectrum measured from

an individual A-line may have sharp fluctuations due to the random nature of the scatterer spacing in the medium and noise.[20] Averaging will yield a better overall description of the scatterer statistical properties by reducing the noise. The average measured backscattered power spectrum (W_{meas}) is given by[15]

$$(4)\quad W_{\text{meas}}(f) = \frac{1}{N}\frac{\Re^2}{4}\sum_{n=1}^{N}\frac{\left|FT\{p_n(t)\}\right|^2}{W_{\text{ref}}(f)},$$

where $\Re$ is the reflection coefficient of the known planar reflector; $FT\{p_n(t)\}$ represents the Fourier transform of the gated RF signal of the nth A-line; N is the number of gated A-lines, and $W_{ref}(f)$ is the calibration power spectrum. The effects of the equipment on the power spectrum measurement are factored out by dividing by a calibration spectrum.[3,15]

The averaged backscattered power spectrum describes the frequency dependence of the scatterers in the medium. Frequency-dependent attenuation will affect the averaged backscattered power spectrum and, if not compensated for, will give rise to inaccurate estimates of scattering properties. To give the most accurate estimates of scattering properties, the frequency-dependent attenuation must be compensated. Attenuation compensation functions exist that account for frequency-dependent losses to the measured power spectrum obtained from gates of finite length.[21–23] The compensated power spectrum (W_{comp}) is represented by

$$(5)\quad W_{\text{comp}}(f) = W_{\text{meas}}(f)A(f,L),$$

where L is the gate length, and $A(f,L)$ is an attenuation compensation function. An attenuation compensation function derived for gated signals by using the Hanning window was used in this study and is given by[23]

$$(6)\quad A(f,L) = e^{4\alpha_0(f)x_0}\left[\frac{2\alpha(f)L}{1-e^{-2\alpha(f)L}}\right]^2 \left[1+\left(\frac{2\alpha(f)L}{2\pi}\right)^2\right]^2,$$

where $\alpha_0(f)$ and x_0 are the attenuation and propagation distance of the intervening tissues, and $\alpha(f)$ is the attenuation coefficient in the gated region (assumed constant).

Estimates of the scatterer properties were made by comparing the logarithm of the compensated, averaged backscattered power spectrum (Eq. 5) with the logarithm of the theoretical power spectrum (Eq. 3)[24]:

$$(7)\quad 10\log_{10} W_{comp}(f) \approx 10\log_{10} f^4 + m(a_{\text{eff}})f^2 + b(n_z, a_{\text{eff}}).$$

Subtracting from both sides of Equation 7 and letting $x = f^2$ yields

$$(8)\quad 10\log_{10} W_{\text{comp}}(x) - 10\log_{10} x^2 \approx m(a_{\text{eff}})x + b(n_z, a_{\text{eff}}).$$

Equation 8 describes a straight line where the slope, m, is a function of the average effective scatterer radius, and the intercept, b, is a function of both the average effective scatterer radius and acoustic concentration. To obtain the scatterer estimates, the least squares method is used to find the best fit slope and intercept to the linearized, average backscattered power spectrum.[24]

Data Acquisition

Spontaneous mammary tumors that had developed in 8 Sprague Dawley rats (Harlan, Indianapolis, IN) were evaluated. The experimental protocol was approved by the campus Laboratory Animal Care Advisory Committee and satisfied all campus and National Institutes of Health rules for the humane use of laboratory animals. Each rat was killed with carbon dioxide, and the tumor and surrounding area were immediately shaved with electric clippers and depilated (Nair; ArmKel, LLC, Princeton, NJ). The rat was then placed on a holder in a tank of degassed water at 37°C for scanning with an ultrasonic transducer.

A weakly focused single-element transducer was used to scan laterally across the tumors and surrounding tissues. The transducer had an aperture diameter of 12 mm and a focal length of 50 mm. The center frequency of the transducer was around 8 MHz with a –6-dB pulse echo frequency bandwidth of about 7 MHz. Estimates of scatterer properties were made within the depth

of focus of the transducer. The center frequency and bandwidth were chosen on the basis of the expected values of the average scatterer sizes in the rat tissues. Insana and Hall[15] showed that the best estimates of scatterer properties were made when the *ka* value (*k* was the acoustic wave number, and *a* was the average scatterer radius) was between 0.5 and 1.2.

The transducer was operated in pulse-echo mode through a pulser/receiver (5800; Panametrics, Waltham, MA). The signals were recorded and digitized on an oscilloscope (9354 TM; LeCroy, Chestnut Ridge, NY) and downloaded to a personal computer for postprocessing. The sampling rate was 50 MHz. Figure 1 shows a rat in a holder ready to be scanned. The mammary tumor is located on the upper left portion of the chest. The black line across the tumor and chest represents the direction and length of the lateral scan. The transducer was moved laterally across the chest and tumor by a micropositioning system with a step size of 100 μm between each A-line scan. The assumed attenuation was 0.9 dB · cm^{-1} · MHz^{-1}. The large attenuation value was based on reports of attenuation measurements in the chest walls of rats and mice.[25]

Figure 1. Rat to be scanned in a holder in a tank of degassed water. Ultrasonic scans ran laterally across the chest and tumor following along the black line. The tumor is located on the upper left side of the chest.

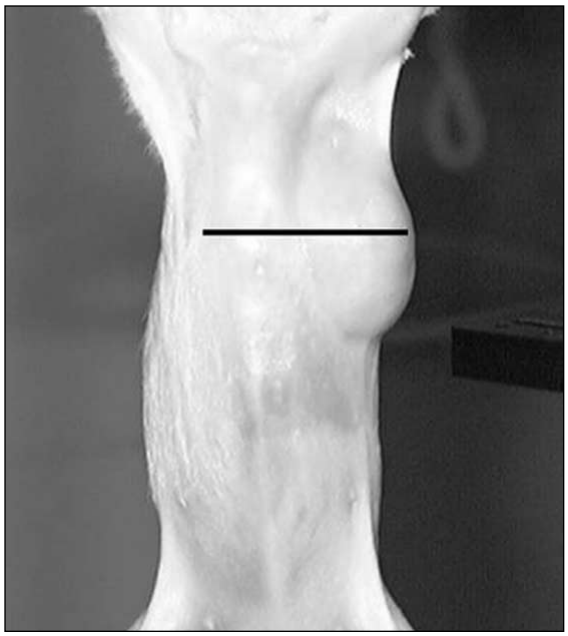

After scanning, the tumors were excised, fixed in 10% neutral-buffered formalin, processed, and stained with hematoxylin-eosin stain for routine histologic evaluation by light microscopy. The tumors were diagnosed as fibroadenomas after histopathologic evaluation. Figure 2 is a photomicrograph of a tissue slice through a tumor viewed on light microscopy. The tumor consisted of well-differentiated epithelial cells arranged in acini surrounded by bands of fibrous connective tissue.

Construction of Parametric Images

Two-dimensional B-mode images were constructed from the ultrasonic scan lines from each rat. Each scan line was taken from a rectangular gated portion of the RF backscattered signal and recorded for postprocessing. From the two-dimensional B-mode images, ROIs were divided into regions inside and outside the tumor where the B-mode images appeared to be homogeneous (no interfaces or large echoes). The regions scanned and analyzed outside the tumors were the first few millimeters of intercostal tissues (normal mammary gland and subcutaneous adipose tissue). The ROIs were separated to determine whether normal surrounding tissues could be differentiated from the tissues inside the tumors on the basis of the scatterer properties. Scatterer properties were compared inside and outside the tumors, because there is an abrupt transition between

Figure 2. Photomicrograph of a rat mammary tumor. The specimen was fixed in 10% neutral buffered formalin, dehydrated, embedded in paraffin, mounted on a glass slide, and stained with hematoxylin-eosin for microscopic evaluation. The tumor consists of well-differentiated epithelial cells arranged in acini surrounded by bands of fibrous connective tissue. The scale bar represents 50 μm.

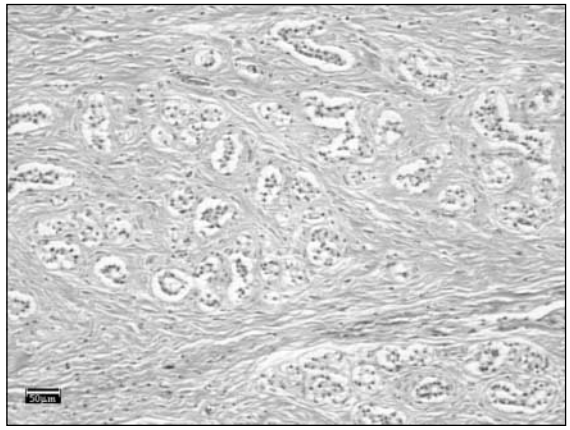

the relatively homogenous tissue located outside the tumor and the tumor itself. Fibroadenomas are well encapsulated (surrounded by collagen) tumors that are relatively heterogeneous internally and heterogeneous when compared with tissues outside the tumor.

The RF echoes were gated from each ROI with the use of a sliding Hanning window with a 75% overlap. Each ROI was a square of 4×4 mm on a side. The side lengths of the ROIs were chosen so that the length of the gated signal would be longer than 10 wavelengths of the center frequency. Topp et al[14] showed that estimated spectrum parameters were independent of gate length when the length of the gated signal was at least 10 wavelengths of the center frequency in the analysis bandwidth.

Scatterer property estimates were made for each ROI by using the best fit line estimation scheme for the Gaussian form factor model (Eq. 8).[24] With the use of a Hanning window with a 75% overlap for each ROI, distinct regions of 1×1 mm were defined with corresponding scatterer property estimates. Each 1×1-mm square was converted to a color pixel according to the estimates of scatterer properties in that square region. The color pixels were then superimposed on the gray scale B-mode images of the rats to create parametric images. Color bars were also displayed next to the parametric images to show the relationship between the color pixels and the scatterer property estimates.

After each parametric image was constructed, the mean values of scatterer property estimates inside and outside the tumor were calculated. The mean of the scatterer property estimates was taken from the first 0.5 cm of tissues. Taking estimates from the first 0.5 cm gave the best overall estimates because it reduced the effects of noise and possible incorrect assumption of the attenuation on the estimates. A statistical comparison between scatterer property estimates inside and outside the tumor was performed by analysis of the variance (single factor); statistical significance was assumed at the $P = .05$ level.

Results

As examples, conventional gray scale B-mode images of rats 2 and 3 and their respective tumors are shown in Figure 3. In Figure 3, the transducer was located above the image facing downward. The transducer was scanned laterally across the chest from the left to the right side. In Figure 3A (rat 2), the tumor is located on the right side of the B-mode image, and the area of the tumor is indicated on the image by white arrows. In Figure 3B (rat 3), the tumor is located on the left side of the B-mode image with the tumor area indicated by white arrows.

Figure 4 shows the 2 parametric images of rat 2 with the tumor. Figure 4A is a parametric image showing the estimated average scatterer diameters. Figure 4B shows a parametric image of the estimated average acoustic concentration. Figure 5 shows the parametric images of rat 3 with the tumor. The color bars relate the estimated average scatterer properties for each ROI to the color of the pixels in the parametric image.

The scatterer property estimates were averaged and compared to assess whether there was a significant difference within the tumors versus the surrounding tissues. Figure 6A shows a chart of the average of the estimated scatterer diameters

Figure 3. Conventional gray scale B-mode images of chest walls and mammary tumors in rats 2 and 3. **A**, The tumor in rat 2 is located on the right side between 1.2 and 3.5 cm on the lateral axis. **B**, The tumor in rat 3 is located on the left side between 0 and 2 cm on the lateral axis. The white arrows indicate the boundaries of the tumors.

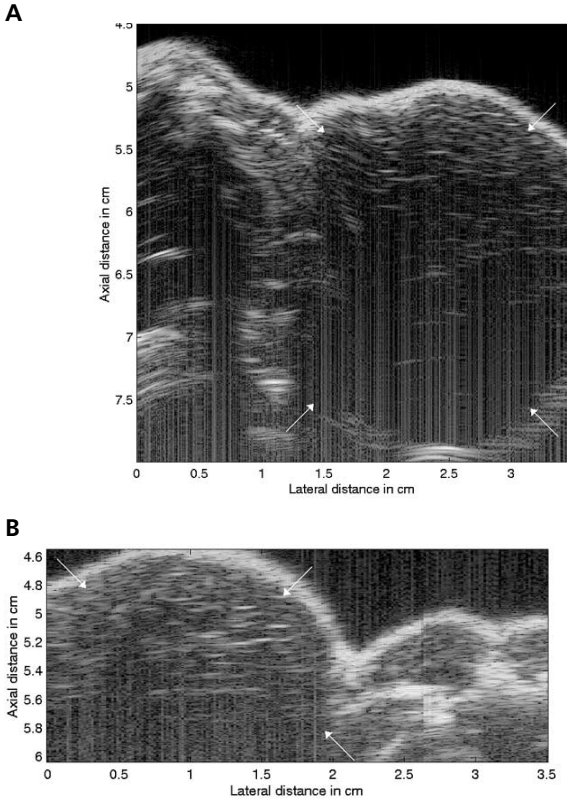

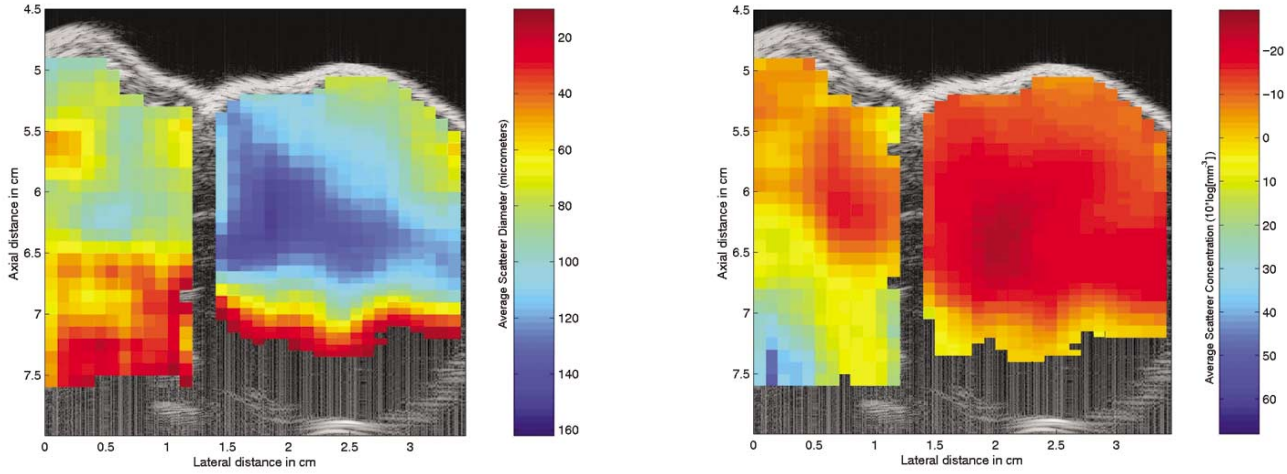

A B

Figure 4. Parametric B-mode image of the chest wall and mammary tumor in rat 2 enhanced by average scatterer diameter estimates (**A**) and average scatterer acoustic concentration estimates (**B**) from a Gaussian form factor model.

for ROIs inside the tumor and for ROIs in surrounding normal tissues. Statistically significant differences between scatterer diameter estimates inside and outside the tumors were seen for rats 2, 3, 5, 6, and 8 but not for rats 1, 4, and 7 ($P = .26$, .45, and .67, respectively). Overall, the average of the scatterer sizes estimated in ROIs outside the tumors was 30% less than the average of scatterer sizes estimated in ROIs inside the tumors.

Figure 6B gives the average of the acoustic concentrations from ROIs in tissues inside and outside the tumors. Statistically significant differences between scatterer acoustic concentration estimates inside and outside were seen for all rats except rat 1 ($P = .87$). The estimated scatterer acoustic concentration was less inside the tumors than outside the tumors. The differences suggested the possibility of making a diagnosis of the tumor state on the basis of the scatterer information and tissue microstructure contained in the enhanced B-mode images.

Figure 5. Parametric B-mode image of the chest wall and mammary tumor in rat 3 enhanced by average scatterer diameter estimates (**A**) and average scatterer acoustic concentration estimates (**B**) form a Gaussian form factor model.

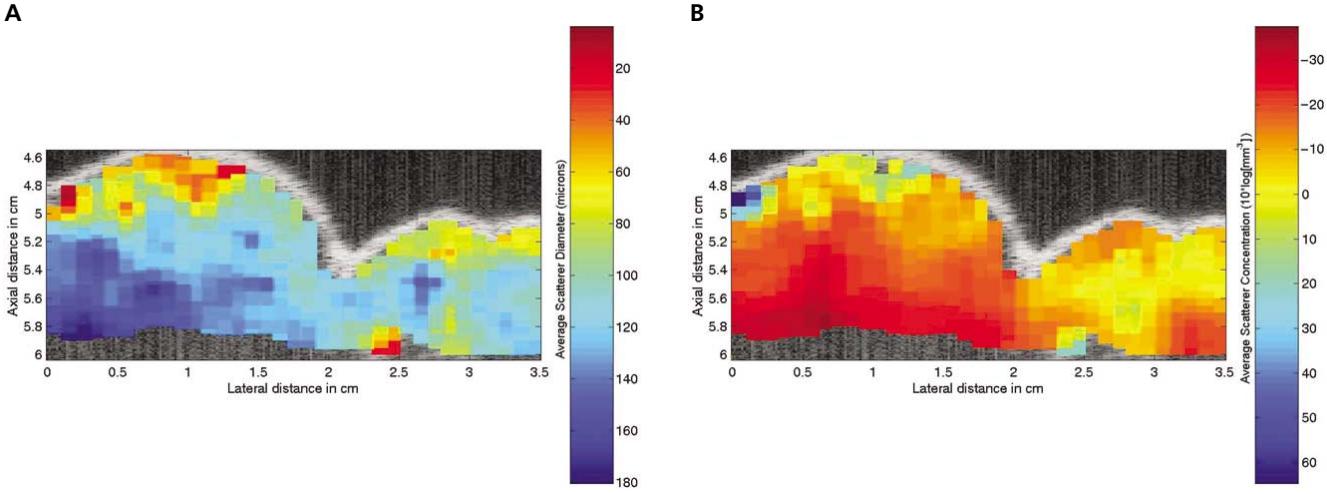

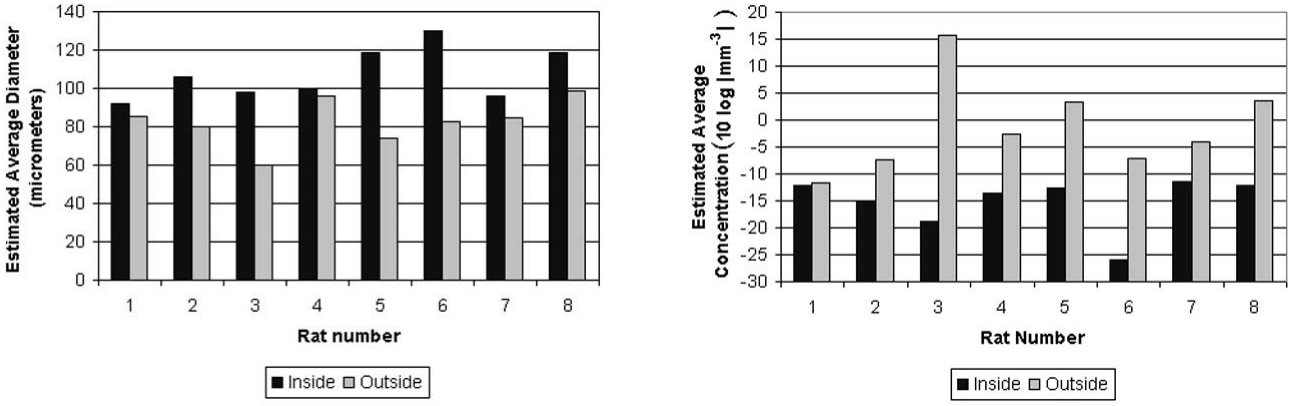

A B

Figure 6. Histograms of average estimated scatterer diameters (**A**) and average estimated scatterer acoustic concentrations (**B**) inside and outside the rat tumors.

The difference between scatterer property estimates made inside and outside the tumor is best seen in the feature analysis graph of Figure 7. Figure 7 plots the average scatterer acoustic concentration versus the average scatterer diameter for the rats inside and outside the tumors. Estimates inside the tumors are located toward the top left quadrant of the graph, whereas estimates made outside the tumors tend to be located in the bottom right quadrant of the graph. On the basis of the estimated feature analysis, the distinction between estimates made inside and outside the tumors can be clearly seen.

Qualitative comparisons between acoustic estimates of the scatterer properties and histologic sections were made from photomicrographs of the tumors. Ultrasonic waves show differences in the mechanical properties of the tissues, whereas light microscopy with staining enables one to visualize the tissue detail directly. Scattering particles are expected to have both mechanical and electromagnetic differences with surrounding tissues. There will not be a one-to-one correlation between mechanical and electromagnetic property changes in the scattering particles, but the optical characteristics should give an approximation of the shape and size that can be related to acoustic estimations. It appears from preliminary qualitative comparisons that the tissue microstructures imaged within the tumors correspond to glandular acini (≈50–150 μm in diameter). Individual cells within these acini are approximately 10 to 20 μm in diameter.

Figure 7. Feature analysis plot of the average scatterer acoustic concentration versus the average scatterer diameter for estimates made inside and outside the tumors.

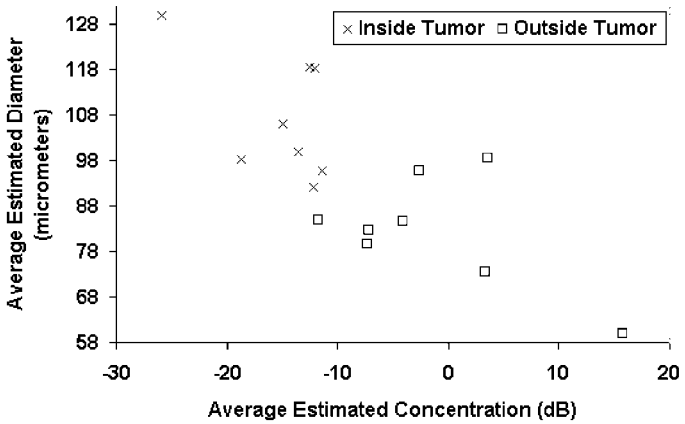

Discussion

In this study, 8 rats with spontaneous mammary tumors were examined sonographically, and estimates of properties of the tissue microstructure were made from the frequency dependence of the backscatter. Parametric images were constructed that superimposed color-coded pixels related to the estimates of the scatterer properties of the average scatterer diameter and acoustic concentration. The study was conducted to show the feasibility of characterizing different tissues on the basis of the estimated scatterer properties. Furthermore, by estimating physical scatterer properties, a limited comparison between sonographic parametric images and light microscopic images was made.

In the case of each rat, the average scatterer diameters estimated inside the tumors were greater than the estimated diameters outside the tumors. In most of the cases, these differences were statistically significant. The comparison of the average scatterer acoustic concentration inside and outside the tumors showed that in each case, the acoustic concentration was greater outside the tumors than inside the tumors. Only 1 case was not shown to be significantly different. The differences suggest that measurement of the estimated scatterer properties may be useful in discerning between different tissue types.

The estimates of the average scatterer diameter depend on the frequency shape of the backscattered power spectrum. The dependence of scatterer diameter estimates on the shape of the power spectrum suggests that accurate compensation of frequency-dependent attenuation is important.

This study has shown that it may be possible to improve the resolution of conventional B-mode scanners, in a statistical sense, through parametric imaging of the tissue microstructure (average scatterer sizes and acoustic concentrations). Furthermore, estimates of the scatterer properties may be verifiable through independent optical means. The study of parametric imaging of the rats and their tumors by quantification of real physical properties of the microstructure is an important step in making parametric imaging a useful alternative to noninvasive diagnosis of disease.

References

1. O'Donnell M, Mimbs JW, Miller JG. Relationship between collagen and ultrasonic backscatter in myocardial tissue. J Acoust Soc Am 1981; 69:580–588.
2. Nicholas D. Evaluation of backscattering coefficients for excised human tissues: results, interpretation and associated measurements. Ultrasound Med Biol 1982; 8:17–28.
3. Lizzi FL, Greenbaum M, Feleppa EJ, Elbaum M. Theoretical framework for spectrum analysis in ultrasonic characterization. J Acoust Soc Am 1983; 73:1366–1373.
4. Nassiri DK, Hill CR. The use of angular scattering measurements to estimate structural parameters of human and animal tissues. J Acoust Soc Am 1986; 79:2048–2054.
5. Insana MF, Wood JG, Hall TJ. Identifying acoustic scattering sources in normal renal parenchyma in vivo by varying arterial and ureteral pressures. Ultrasound Med Biol 1991; 17:613–626.
6. Chivers RC, Hill CR. A spectral approach to ultrasonic scattering from human tissue: methods, objectives and backscattering measurements. Phys Med Biol 1975; 20:799–815.
7. Feleppa EJ, Lizzi FL, Coleman DJ, Yaremko MM. Diagnostic spectrum analysis in ophthalmology: a physical perspective. Ultrasound Med Biol 1986; 12:623–631.
8. Lizzi FL, Ostromogilsky M, Feleppa EJ, Rorke MC, Yaremko MM. Relationship of ultrasonic spectral parameters to features of tissue microstructure. IEEE Trans Ultrason Ferroelectr Freq Control 1986; 33: 319–329.
9. Shung KK, Thieme GA. Ultrasonic Scattering in Biological Tissues. Boca Raton, FL: CRC Press; 1993.
10. Golub RM, Parsons RE, Sigel B, et al. Differentiation of breast tumors by ultrasonic characterization. J Ultrasound Med 1993; 12:601–608.
11. Zagzebski JA, Lu ZF, Xao LX. Quantitative ultrasound imaging: in vivo results in normal liver. Ultrason Imaging 1993; 15:335–351.
12. Feleppa EJ, Liu T, Kalisz A, et al. Ultrasonic spectral-parameter imaging of the prostate. Int J Imaging Syst Technol 1997; 8:11–25.
13. Lizzi FL, Astor M, Liu T, Deng C, Coleman DJ, Silverman RH. Ultrasonic spectrum analysis for tissue assays and therapy evaluation. Int J Imaging Syst Technol 1997; 8:3–10.
14. Topp KA, Zachary JF, O'Brien WD Jr. Quantifying B-mode images of in vivo rat mammary tumor with frequency dependence of backscatter. J Ultrasound Med 2001; 20:605–612.
15. Insana MF, Hall TJ. Parametric ultrasound imaging from backscatter coefficient measurements: image formation and interpretation. Ultrason Imaging 1990; 12:245–267.
16. Insana MF, Hall TJ, Wood JG, Yan ZY, Renal ultrasound using parametric imaging techniques to detect changes in microstructure and function. Invest Radiol 1993; 28:720–725.

17. Insana MF. Modeling acoustic backscatter from kidney microstructure using an anisotropic correlation function. J Acoust Soc Am 1995; 97:649–655.

18. Faran JJ Jr. Sound scattering by solid cylinders and spheres. J Acoust Soc Am 1951; 23:405–418.

19. Insana MF, Wagner RF, Brown DG, Hall TJ. Describing small-scale structure in random media using pulse-echo ultrasound. J Acoust Soc Am 1990; 87:179–192.

20. Wear KA, Wagner RF, Insana MF, Hall TJ. Application of autoregressive spectral analysis to cepstral estimation of mean scatterer spacing. IEEE Trans Ultrason Ferroelectr Freq Control 1993; 40:50–58.

21. Sigelmann RA, Reid JM. Analysis and measurement of ultrasound backscattering from an ensemble of scatterers excited by sine-wave bursts. J Acoust Soc Am 1973; 53:1351–1355.

22. O'Donnell M, Miller JG. Quantitative broadband ultrasonic backscatter: an approach to nondestructive evaluation in acoustically inhomogeneous materials. J Appl Phys 1981; 52:1056–1065.

23. Oelze ML, O'Brien WD Jr. Frequency-dependent attenuation-compensation functions for ultrasonic signals backscattered from random media. J Acoust Soc Am 2002; 111:2308–2319.

24. Oelze ML, Zachary JF, O'Brien WD Jr. Characterization of tissue microstructure using ultrasonic backscatter: theory and technique optimization using a Gaussian form factor. J Acoust Soc Am 2002; 112:1202–1211.

25. Teotica GA, Miller RJ, Frizzell LA, Zachary JF, O'Brien WD Jr. Attenuation coefficient estimates of mouse and rat chest wall. IEEE Trans Ultrason Ferroelectr Freq Control 2001; 48:593–600.